

5-1-2001

Oxygen Permeation Through Cobalt-Containing Perovskites: Surface Oxygen Exchange vs. Lattice Oxygen Diffusion

Kevin Huang

University of South Carolina - Columbia, huang46@cec.sc.edu

John B. Goodenough

Follow this and additional works at: https://scholarcommons.sc.edu/emec_facpub



Part of the [Mechanical Engineering Commons](#)

Publication Info

Published in *Journal of The Electrochemical Society*, Volume 148, Issue 5, 2001, pages E203-E214.

This Article is brought to you by the Mechanical Engineering, Department of at Scholar Commons. It has been accepted for inclusion in Faculty Publications by an authorized administrator of Scholar Commons. For more information, please contact digres@mailbox.sc.edu.



Oxygen Permeation Through Cobalt-Containing Perovskites Surface Oxygen Exchange vs. Lattice Oxygen Diffusion

Keqin Huang,^{a,*} and John B. Goodenough

Texas Materials Institute, The University of Texas at Austin, Austin, Texas 78712, USA

The oxygen permeation fluxes from p'_{O_2} to p''_{O_2} ($p'_{O_2} > p''_{O_2}$) across cobalt-containing perovskite ceramic membranes $La_{1-x}Sr_xCoO_{3-\delta}$ and $SrCo_{0.8}Fe_{0.2}O_{3-\delta}$ were measured by gas chromatography as functions of oxygen chemical potential gradient, temperature, thickness, and catalytic activity on the surface. Power indexes $0.5 > n > 0$ for uncatalyzed $La_{1-x}Sr_xCoO_{3-\delta}$ and $1 > n > 0.5$ for $SrCo_{0.8}Fe_{0.2}O_{3-\delta}$ were obtained when J_{O_2} vs. $p'^n_{O_2} - p''^n_{O_2}$ was plotted as a straight line. The results clearly indicate an overall permeation process controlled by both surface oxygen exchange and bulk oxygen diffusion for uncatalyzed $La_{1-x}Sr_xCoO_{3-\delta}$ and $SrCo_{0.8}Fe_{0.2}O_{3-\delta}$. Application of a thin layer of catalytically active $SrCo_{0.8}Fe_{0.2}O_{3-\delta}$ on the feeding-gas surface of $La_{0.5}Sr_{0.5}CoO_{3-\delta}$ under the condition of a fixed $p'_{O_2} = 0.21$ atm and a varied p''_{O_2} not only increases remarkably the overall oxygen flux, but also changes a mixed control to a bulk diffusion control. This enables evaluation of the bulk transport properties of the mixed conductors. A coat of $SrCo_{0.8}Fe_{0.2}O_{3-\delta}$ on the permeate side has little catalytic effect, especially at low p''_{O_2} range, due to the formation of a poorly conducting brownmillerite phase. The results explicitly show a higher activation energy for the surface exchange kinetics than for the ambipolar transport in the mixed conductors. The mechanism of the surface exchange is discussed, and an analytic expression that agrees well with the experimental results is obtained.
© 2001 The Electrochemical Society. [DOI: 10.1149/1.1362548] All rights reserved.

Manuscript submitted May 18, 2000; revised manuscript received January 20, 2001.

Dense ceramic membranes exhibiting a high electronic and oxide-ion conductivity have attracted increasing attention in recent years since eventual commercialization of the chemical reactors based on these membranes provides an economic, clean, and efficient means to separate oxygen from ambient air or other oxygen-containing atmospheres. The success of this technology could possibly revolutionize the present chemical industry that manufactures the oxygen and synthetic gas ($H_2 + CO$) expensively. Theoretically, mixed electronic and oxide-ion conduction is an important transport phenomenon in oxide systems. A profound understanding of the transport mechanisms not only helps to establish physical models for practical oxygen reactors, but also provides criteria to find new families of mixed electronic and oxide-ion conductors.

Determination of oxide-ion conductivity in mixed conducting oxides is critical to a fundamental understanding of these materials. However, most promising mixed conductors, such as those with perovskite structure, possess a dominant electronic conductivity with a small component of oxide-ion conductivity. Therefore, a simple van der Pauw four-probe method only reveals the electronic conductivity because the oxygen flux is too small to be measured. Although numerous studies¹⁻³ have made considerable effort to separate oxide-ion conductivity by ion-blocking and/or electron-blocking methods, the experimental procedure appears to be complicated and the data lack reliability and reproducibility.

Maier⁴ has summarized three basic methods for studying oxide-ion transport in the oxide systems: electrical, isotope tracer, and chemical-gradient measurements. In the electrical measurement, represented by the van der Pauw method, an external electrical field ($\nabla\phi$) is applied across the sample as a driving force. The internal electronic and/or oxide-ion current is balanced by an external electronic current, and Ohm's law prevails. The resulting conductivity thereby includes both electronic and/or oxide-ion conductivity. However, it is very difficult to separate a small fraction of oxide-ion conductivity from an electronically dominated total conductivity within the tolerance of experimental error. In this case, the measurement provides primarily information on the electrons. In the isotope-tracer measurement, the surface of the sample is exposed to an atmosphere containing an isotope of oxygen ^{18}O . The ^{18}O diffuses

into the sample as a result of the existing ^{18}O chemical gradient [$\nabla\mu(^{18}O)$] with the ^{18}O ionic flux being internally balanced by the ionic flux of its counter isotope ^{16}O . In this case, Fick's law governs the diffusional process. By fitting the measured ^{18}O profiles across the sample surface, the oxygen exchange coefficient k_s and the isotope oxygen diffusivity D_o^* can be obtained simultaneously. Many studies in this area have been carried out by Steele and Kilner.⁵⁻⁹ In the third method, the gradient of the chemical potential of oxygen [$\nabla\mu(O_2)$] across a mixed conducting oxide is the driving force for the oxygen diffusion. Different from the first two measurements, a true gradient of the chemical potential of oxygen is involved, and the oxide-ion flux is internally compensated by the electronic flux provided an ambipolar conduction prevails in the oxides. Therefore, a measure of oxide-ion flux could possibly offer a greater and better opportunity to determine oxide-ion conductivity since only oxide ions contribute to the permeation process in the presence of a pool of electrons. More studies¹⁰⁻¹² have focused on this method to obtain the oxide-ion conductivity in electron-dominated mixed conductors. However, the prerequisite for this method is a lattice oxygen diffusion that rate-determines the overall permeation process. Any involvement of slow surface oxygen exchange could undervalue the measured oxide-ion conductivity. This is especially true where thinner ceramic membranes are utilized in the permeation cell.

The technological significance of surface exchange kinetics has been increasingly realized in recent years,¹³⁻¹⁵ but a detailed description of the exchange process for oxide systems in terms of an exact reaction mechanism on an atomic scale, rate-determining steps, and adsorption site is still lacking. Steele¹³ and Bouwmeester *et al.*¹⁴ have both stressed the importance of surface exchange kinetics in determining the oxygen flux through oxide-ion conducting membranes. To obtain a high oxygen flux J_{O_2} , it is desirable to have a thin membrane as indicated by the Wagner equation applicable where bulk oxygen diffusion dominates

$$J_{O_2} = -\frac{RT}{16F^2L} \int_{p''_{O_2}}^{p'_{O_2}} \frac{\sigma_o \sigma_e}{\sigma_o + \sigma_e} d \ln p_{O_2} \quad [1]$$

where p'_{O_2} and p''_{O_2} are the partial pressures of oxygen of feeding gas and sweeping gas, respectively, σ_o and σ_e are the oxide-ion and electronic conductivities, respectively, and $\sigma_o \sigma_e / (\sigma_o + \sigma_e) = \sigma_{ambi}$ is the ambipolar conductivity. L is the thickness of the membrane; R , T , and F have their usual meanings.

* Electrochemical Society Student Member.

^a Present address: Siemens Westinghouse Power Corporation, Pittsburgh, Pennsylvania 15235, USA.

^z E-mail: keqin.huang@swpc.siemens.com

Table I. Final sintering temperatures for $\text{La}_{1-x}\text{Sr}_x\text{CoO}_{3-\delta}$ and $\text{SrCo}_{0.8}\text{Fe}_{0.2}\text{O}_{3-\delta}$.

Samples	Sintering temperature ($^{\circ}\text{C}$)	Duration (h)
$\text{La}_{1-x}\text{Sr}_x\text{CoO}_{3-\delta}$		
$x = 0.20$	1300	15
$x = 0.40$	1300	15
$x = 0.50$	1270	15
$x = 0.60$	1250	15
$x = 0.70$	1230	15
$\text{SrCo}_{0.8}\text{Fe}_{0.2}\text{O}_{3-\delta}$	1200	15

However, at or below the critical thickness $L_c = D_o^*/k_s$ as defined by Bouwmeester *et al.*,¹⁴ the surface exchange kinetics limits the oxygen flux. No further oxygen flux gain is achieved by making the membranes thinner. Note that the oxygen exchange kinetics at a gas-solid interface plays a fundamental role in the catalytic activity of the material. A correlation between oxygen exchange kinetics and catalytic activity has been established.^{16,17} A catalytic surface layer on a studied membrane could change the kinetics from surface exchange control to lattice diffusion control.

Of the known mixed conductors, the cobalt-containing oxides with perovskite structure have been most extensively studied because of their extremely high oxygen permeation rate at elevated temperatures; their potential applications are as ceramic membranes of chemical reactors and cathodes of a solid oxide fuel cell. In this paper, we report systematic measurements of the oxygen permeation fluxes through membranes of selected cobalt-containing perovskites by gas chromatography (GC). The results clearly indicate a mixed control over the total permeation rate by surface oxygen exchange and bulk oxygen diffusion. With a porous catalytic surface layer, the studied perovskite exhibits a changeover from mixed surface and bulk control to bulk control. The mechanisms for oxygen exchange kinetics on an atomic scale are discussed to interpret the results.

Experimental

Preparation of samples.—The studied samples have a formula $\text{La}_{1-x}\text{Sr}_x\text{CoO}_{3-\delta}$ (LSCo) where $x = 0.2, 0.4, 0.5, 0.6,$ and 0.7 . The samples with $x > 0.7$ were not investigated because they do not have a perovskite structure. The Pechini method was used to synthesize the $\text{La}_{1-x}\text{Sr}_x\text{CoO}_{3-\delta}$ compounds. Details about this method are described in Ref. 18 and 19. The decomposed ceramic powders were ballmilled to break up the soft agglomerates and pressed into 1 in. diam pellets under 200 MPa pressure. The final sintering temperatures and duration for each composition are listed in Table I. For comparison, $\text{SrCo}_{0.8}\text{Fe}_{0.2}\text{O}_{3-\delta}$ (SCF) was also made in this study by solid-state reaction. The powders were ground three times after each 1000 $^{\circ}\text{C}$ calcination and finally sintered at 1200 $^{\circ}\text{C}$ for 15 h.

Whether lattice oxygen diffusion or surface oxygen exchange limits the overall permeation rate through a mixed ionic and electronic conductor (MIEC) is primarily determined by the relative magnitude of the rates of lattice diffusion and surface exchange. To enhance the rate of reaction at the surfaces of LSCo samples so as to make lattice oxygen diffusion the rate-determining step, a thin layer of SCF, which has been reported previously to have the highest oxygen permeation flux among the MIECs discovered,^{20,21} was applied directly by pasting an SCF ink either on one surface of LSCo or on both. The SCF ink was made by thoroughly mixing fine SCF powders with organic binder (V-6 manufactured by Heraeus Inc.), terpineol, and oleic acid in a certain ratio. The coated LSCo was then fired at 1200 $^{\circ}\text{C}$ for 30 min to increase the bonding between the coating and substrate. From our previous experience, the microstructures of the coating resulting from the above ink are mesoporous.

Powder X-ray diffraction (XRD) was performed on a PW 1740 diffractometer from 10 to 80 $^{\circ}$ with Cu K α radiation and a Ni filter.

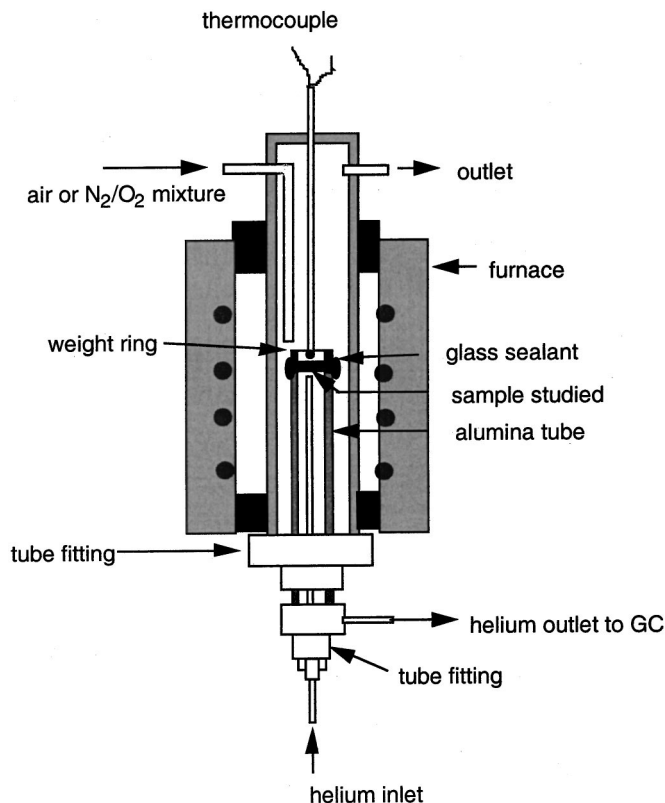


Figure 1. Experimental setup for oxygen permeation measurements.

Synthetic silicon powder as an internal standard was used for determining the lattice parameters. From the XRD patterns, the structures and the related lattice parameters were determined with Rietveld refinement.

Oxygen permeation measurement.—The aforementioned sintered pellets, which usually shrank to ~ 0.7 in. diam, were first ground on both sides with a diamond wheel to a desired thickness. The grinding also ensured removal of possibly contaminated surface layers. The fresh pellets thus obtained were then mounted on the top of a supporting alumina tube with a glass ring that was covered with a glass-powder slurry to ensure further sealing. An alumina ring (the same size as the supporting tube) on the top of the sample was also used as a weight to keep the seal leak-tight while maintaining the same permeation area on both sides of the sample. To eliminate the edge effect (extra oxygen permeation through uncounted area), the outer glass-powder slurry covers the overall edges of the sample. The whole setup of the permeation cell is illustrated in Fig. 1. The assembly was then loaded into the constant-temperature zone of a vertical furnace and slowly heated to 900–950 $^{\circ}\text{C}$ to allow the glass to soften and seal the assembly. The measurement proceeded in a cooling sequence.

GC with a 5 \AA molecular-sieve column and a thermal conductivity detector was used to measure the oxygen contents in the sweeping helium (purity $>99.999\%$) because simultaneously measuring the nitrogen content can monitor the leak-tightness of a permeation cell. The oxygen concentration in the sweeping helium was measured at a given flow rate, and ambient air or an $\text{N}_2\text{-O}_2$ mixture at a flow rate of 45 mL/min was used as the feeding gas at the other side of the permeation cell. A special six-port Valco valve was employed to inject the sample gas into an SRI 8610C GC when needed. PeakSimple software was used to collect and analyze the data by integrating the individual peak areas corresponding to either oxygen or nitrogen. The column was calibrated usually once a month with He-0.1% O_2 and He-1% O_2 mixtures as the standard

Table II. Lattice parameters of $\text{La}_{1-x}\text{Sr}_x\text{CoO}_{3-\delta}$ and $\text{SrCo}_{0.8}\text{Fe}_{0.2}\text{O}_{3-\delta}$.

Samples	Symmetry	$a(r)$ (Å)	$\alpha(r)^{(o)}$
$\text{La}_{1-x}\text{Sr}_x\text{CoO}_{3-\delta}$			
$x = 0.2$	Rhombohedral	3.836(4)	90.48
$x = 0.4$	Rhombohedral	3.835(4)	90.23
$x = 0.5$	Rhombohedral	3.833(4)	90.14
$x = 0.6$	Cubic	3.834(1)	90.00
$x = 0.7$	Cubic	3.837(1)	90.00
$\text{SrCo}_{0.8}\text{Fe}_{0.2}\text{O}_{3-\delta}$	Cubic	3.853(0)	90.00

gases depending on how heavily the GC was used. For all measurements, the flow rate of the carrier helium gas (purity >99.999%) for carrying effluent (the sweeping gas in a 1 mL sample loop on the valve in this case) into the GC for analysis was 20 mL/min. Any detectable nitrogen was regarded as leakage from air, and the corresponding oxygen content was subtracted from the measured value. If the nitrogen content was above 0.1%, the measurement was abandoned. If the continuously stirred tank reactor condition is satisfied in our permeation cell and the sweeping helium behaves ideally, the oxygen permeation flux J_{O_2} can be calculated from the flow rate of the sweeping gas, the volume fraction of oxygen analyzed by GC, and the effective permeation area.

The variations of chemical potential gradient of oxygen across the MIEC were achieved by either changing the flow rate of the sweeping helium gas while keeping the feeding gas as ambient air ($p'_{\text{O}_2} = 0.21$ atm), or by altering the ratio of O_2 in an N_2 - O_2 mixture as the feeding gas while keeping the flow rate of sweeping helium gas constant, normally 20 mL/min. In the former case, the flow rate of the sweeping helium gas, usually ranging from 5 to 150 mL/min, was regulated by a mass flow controller (MFC), (MKS model 1179A with four-channel readout unit model 247). A smaller flow rate usually requires longer equilibration times. Therefore, at each temperature, the measurement was started from the smallest flow rate and was held overnight to ensure that real equilibrium was achieved. In the latter case, the oxygen content in the feeding gas was changed by varying the flow rates of oxygen and nitrogen, which are also regulated by the MFC. Similar to the former case, the permeation measurement was started from the lowest partial pressure of oxygen, and the cell was held overnight at high temperatures before continuing to the next p_{O_2} . Each measurement takes approximately 8 h at each temperature.

Results and Discussion

Structural changes as a function of Sr content.—The lattice parameters of both $\text{La}_{1-x}\text{Sr}_x\text{CoO}_{3-\delta}$ and $\text{SrCo}_{0.8}\text{Fe}_{0.2}\text{O}_{3-\delta}$ samples are listed in Table II. Consistent results with those reported in the literature²² were obtained. For $x = 0.2, 0.4,$ and 0.5 , the structure is rhombohedral, which distorts from the cubic by an angle $|\alpha(r) - 90^\circ|$. It is apparent from Table II that the extent of distortion decreases with increasing x to $x = 0.5$, above which the structures change to primitive cubic without distortion. The lattice parameter $a(r)$ shows a slight decrease with increasing x , but $\alpha(r)$ exhibits a pronounced monotonous decrease. From the following results, it appears that $\alpha(r)$, and therefore the Co-O-Co bond angle, has a more profound effect on the oxide-ion conductivity than $a(r)$ as is discussed in detail in the section on Mechanisms for both surface oxygen exchange and bulk oxygen diffusion control. Unlike previous reports,^{20,21} a small amount of unknown impurity is consistently found in the primitive cubic matrix of air-annealed $\text{SrCo}_{0.8}\text{Fe}_{0.2}\text{O}_{3-\delta}$ even after several intermediate grindings. How-

ever, it gives a pure primitive cubic phase after annealing in oxygen. The lattice parameters of $\text{SrCo}_{0.8}\text{Fe}_{0.2}\text{O}_{3-\delta}$ shown in Table II were obtained from an oxygen-annealed sample.

Oxygen permeation flux J_{O_2} without catalytic surface layer.—In the following paragraphs, p'_{O_2} and p''_{O_2} denote the partial pressures of oxygen at the feeding and the permeate side, $p'_{\text{O}_2} > p''_{\text{O}_2}$, respectively. Unless especially mentioned, we choose the composition $\text{La}_{0.5}\text{Sr}_{0.5}\text{CoO}_{3-\delta}$ as a representative example of the $\text{La}_{1-x}\text{Sr}_x\text{CoO}_{3-\delta}$ system. Most of the experimental data can be found in Table III.

Previous studies^{23,24} have shown a power law with the index $n < 0$ between oxygen nonstoichiometry δ and the oxygen partial pressure p_{O_2} in the $\text{La}_{1-x}\text{Sr}_x\text{CoO}_{3-\delta}$ system at elevated temperatures. One can then expect, from the Wagner equation with $\sigma_{\text{ambi}} \approx \sigma_{\text{ambi}}^{\text{O}} p_{\text{O}_2}^n$ ($n < 0$), a straight-line plot of J_{O_2} vs. $p'_{\text{O}_2} - p''_{\text{O}_2}$ with $n < 0$, provided the overall permeation is rate determined by bulk oxygen diffusion. The ambipolar conductivity $\sigma_{\text{ambi}} \sim \exp(-E_a/kT)$ can be calculated from the slope of the line by using Wagner's equation.

J_{O_2} under $p'_{\text{O}_2} = 0.21$ atm and varied p''_{O_2} .—The oxygen partial pressure p''_{O_2} in the sweeping helium has a power law relationship with its flow rate F for $\text{La}_{0.5}\text{Sr}_{0.5}\text{CoO}_{3-\delta}$ (see Fig. 2). Since the oxygen flux J_{O_2} is proportional to the product of p''_{O_2} and F , the observed power law relationship implies that J_{O_2} is proportional to $p''_{\text{O}_2}{}^m$ ($m = 1 - 1/s$, $m < 0$) if no cell leakage is considered. It appears to conflict with the results shown in Fig. 5, where a positive power index n in J_{O_2} vs. $p'_{\text{O}_2} - p''_{\text{O}_2}$ is observed. We believe this deviation results from two factors. First, the existence of a certain amount of cell leakage requires using different p''_{O_2} for plotting Fig. 2 (not corrected for air leak) and for calculating J_{O_2} (corrected for air leak). Second, the power index n in J_{O_2} vs. $p'_{\text{O}_2} - p''_{\text{O}_2}$ was obtained by a nonlinear least-squares fitting with the justification of boundary condition of $J_{\text{O}_2} = 0$ at $p'_{\text{O}_2} = p''_{\text{O}_2}$, while no boundary condition is required for the relationship of p''_{O_2} and F shown in Fig. 2.

The temperature dependence of the measured overall oxygen permeation flux at different driving forces $\log(p'_{\text{O}_2}/p''_{\text{O}_2})$ for the composition $\text{La}_{0.5}\text{Sr}_{0.5}\text{CoO}_{3-\delta}$ is illustrated in Fig. 3. By the Wagner equation, this dependence can only be meaningfully established at a given sample thickness and driving force $\log(p'_{\text{O}_2}/p''_{\text{O}_2})$. As clearly shown in the figure, $\log(J_{\text{O}_2})$ vs. $1/T$ at a given driving force yields a straight line; the activation energy E_a for the permeation process can be calculated from the slope. These results are very close to those obtained from the slope of J_{O_2} vs. $p'_{\text{O}_2} - p''_{\text{O}_2}$ shown in Table III, but they depend strongly on the Co-O-Co bond angle and/or Sr-doping level. Note that E_a might not represent a single process; it could include both surface exchange and bulk diffusion.

The J_{O_2} of a $\text{La}_{0.6}\text{Sr}_{0.4}\text{CoO}_{3-\delta}$ membrane of thickness L at a given temperature and driving force $\log(p'_{\text{O}_2}/p''_{\text{O}_2})$ is plotted against $1/L$ in Fig. 4. Although J_{O_2} increases roughly inversely with L for larger L , it is very hard to distinguish the bulk and surface control by this plot because there is no sample thicker than 1.7 mm in this portion of the study, which was intended to reach a critical value L_c . Other compositions gave similar results; even at a thickness of 2.5 mm, a slow surface exchange appears to be controlling for the cobalt-containing perovskites. The concept of the critical length¹⁴ L_c has been proposed by assuming a linearized surface exchange and bulk diffusion at a small p_{O_2} gradient. It may not be applicable in our case.

Table III. Nonlinear least-squares fitting data on $J_{O_2} = \theta (p'_{O_2}{}^n - p''_{O_2}{}^n)$, where $p'_{O_2} = 0.21 \text{ atm}$, $0.21 \text{ atm} > p''_{O_2} > 5 \times 10^{-4} \text{ atm}$. Samples have no catalytic layer SCF on the surface.

Sample	Thickness (mm)	T (°C)	Order (n)	n by TGA (800 °C) ²³	θ (mol cm ⁻² s ⁻¹ atm ⁻ⁿ)	Activation energies (eV)	
La _{1-x} Sr _x CoO _{3-δ} $x = 0.2$	1.30	930	-0.10 ± 0.07	-0.25	2.05 × 10 ⁻⁸	1.78 ± 0.14	
		910	-0.20 ± 0.08		1.66 × 10 ⁻⁸		
		890	-0.30 ± 0.05		1.22 × 10 ⁻⁸		
		870	-0.35 ± 0.09		8.37 × 10 ⁻⁹		
		850	-0.25 ± 0.12		5.40 × 10 ⁻⁹		
	$x = 0.4$	1.70 ^a	930	0.31 ± 0.04	—	3.07 ± 0.04 × 10 ⁻⁷	1.39 ± 0.09
			910	0.21 ± 0.03		2.76 ± 0.13 × 10 ⁻⁷	
			890	0.16 ± 0.03		2.45 ± 0.28 × 10 ⁻⁷	
			850	0.10 ± 0.04		1.85 ± 0.45 × 10 ⁻⁷	
	$x = 0.5$	1.34	930	0.21 ± 0.03	-0.07	3.48 ± 0.17 × 10 ⁻⁷	1.56 ± 0.05
			910	0.25 ± 0.03		3.02 ± 0.07 × 10 ⁻⁷	
			890	0.26 ± 0.03		2.23 ± 0.05 × 10 ⁻⁷	
			870	0.27 ± 0.03		1.61 ± 0.03 × 10 ⁻⁷	
			830	0.23 ± 0.05		9.36 ± 0.04 × 10 ⁻⁸	
			810	0.30 ± 0.06		6.92 ± 0.09 × 10 ⁻⁸	
$x = 0.6$	2.10	950	0.33 ± 0.06	---	7.05 ± 0.16 × 10 ⁻⁷	0.72 ± 0.03	
		930	0.29 ± 0.09		6.48 ± 0.40 × 10 ⁻⁷		
		910	0.34 ± 0.05		5.58 ± 0.08 × 10 ⁻⁷		
		890	0.37 ± 0.02		4.94 ± 0.02 × 10 ⁻⁷		
		870	0.29 ± 0.08		4.52 ± 0.26 × 10 ⁻⁷		
		850	0.25 ± 0.09		3.98 ± 0.46 × 10 ⁻⁷		
		830	0.28 ± 0.08		3.28 ± 0.23 × 10 ⁻⁷		
$x = 0.7$	2.50	910	0.41 ± 0.07	-0.05	7.95 ± 0.26 × 10 ⁻⁷	0.88 ± 0.07	
		890	0.20 ± 0.05		7.67 ± 0.78 × 10 ⁻⁷		
		870	0.24 ± 0.09		6.68 ± 0.75 × 10 ⁻⁷		
		850	0.27 ± 0.10		5.57 ± 0.46 × 10 ⁻⁷		
		830	0.32 ± 0.10		4.55 ± 0.14 × 10 ⁻⁷		
		810	0.41 ± 0.05		3.71 ± 0.08 × 10 ⁻⁷		
		SrCo _{0.8} Fe _{0.2} O _{3-δ}	1.48		930		0.82 ± 0.15
910	0.83 ± 0.20			3.24 ± 0.73 × 10 ⁻⁶			
890	0.89 ± 0.16			3.30 ± 0.65 × 10 ⁻⁶			
870	0.90 ± 0.05			3.07 ± 0.22 × 10 ⁻⁶			
850	0.75 ± 0.09			2.44 ± 0.25 × 10 ⁻⁶			
830	0.78 ± 0.08			2.32 ± 0.22 × 10 ⁻⁶			
810	0.74 ± 0.09			2.01 ± 0.21 × 10 ⁻⁶			

^a Other thicknesses are not shown in this table.

As shown in Table III, an $n < 0$ close to the value obtained by thermogravimetric analysis (TGA) is only observed for the $x = 0.2$ sample. The agreement indicates a bulk diffusion dominating the permeation. The calculated ambipolar conductivity for this composition is $\sigma_O = (3.49 \pm 0.59) \times 10^8 \exp(-1.78 \pm 0.14(\text{eV})/kT)$ from which $\sigma_O \approx 0.01 \text{ S/cm}$ at 930°C is obtained. The low value of σ_O and high value of E_a are due to the presence of a dynamic phase segregation in the $x = 0.2$ composition.²⁵ However, an $n > 0$ is found for the other compositions. Figure 5 presents such a plot for $x = 0.5$ with fitted lines passing through the origin (0, 0). The optimized n by nonlinear least-squares fitting is obtained as $0.5 > n > 0$. If the bulk diffusion is assumed to prevail, then $n > 0$ implies an oxygen interstitial mechanism for the transport of charge carriers. This is impossible for the perovskite structure because there is no possible interstitial position for oxygen in the structure.

Therefore, it is certain that a mixed surface exchange and bulk diffusion control the permeation rate or a sole surface exchange control is responsible for the $n > 0$ as is discussed in the section on Mechanisms. Also, thinner samples yield n much closer to 0.5, which also supports such an assumption. By a similar treatment, $1 > n > 0.5$ has been calculated for O₂ adsorption at Fe³⁺ and is

found in SrCo_{0.8}Fe_{0.2}O_{3-δ}, as shown in Fig. 6. This result disagrees with that in,²⁶ where $n = 0.5$ was claimed. Thus, different mechanisms have been involved for these two types of compounds.

Note that no linear dependence of J_{O_2} on $\log(p'_{O_2}/p''_{O_2})$ that passes through (0, 0) can be found in this study. Determination of oxide-ion conductivity from the slope of the J_{O_2} vs. $\log(p'_{O_2}/p''_{O_2})$ line without justifying at $J_{O_2} = 0$ at $p'_{O_2} = p''_{O_2}$ would contain errors.

J_{O₂} under varied p'_{O_2} and fixed sweeping-gas flow rate.—With a fixed sweeping-gas flow rate, the gradient of the partial pressure of oxygen is determined by variations of both p'_{O_2} and p''_{O_2} , whereas only p''_{O_2} changes as a result of variation of the sweeping-gas flow rate in the experiment with a fixed $p'_{O_2} = 0.21 \text{ atm}$. Comparison of the results from the two types of experiments should reveal the effect of partial pressures of oxygen in the feeding gas and of the flowing patterns of the sweeping gas on the surface reaction kinetics.

The variations of p''_{O_2} as a function of p'_{O_2} are shown in Fig. 7 for a fixed sweeping-gas flow rate of 20 mL/min. All curves taken at

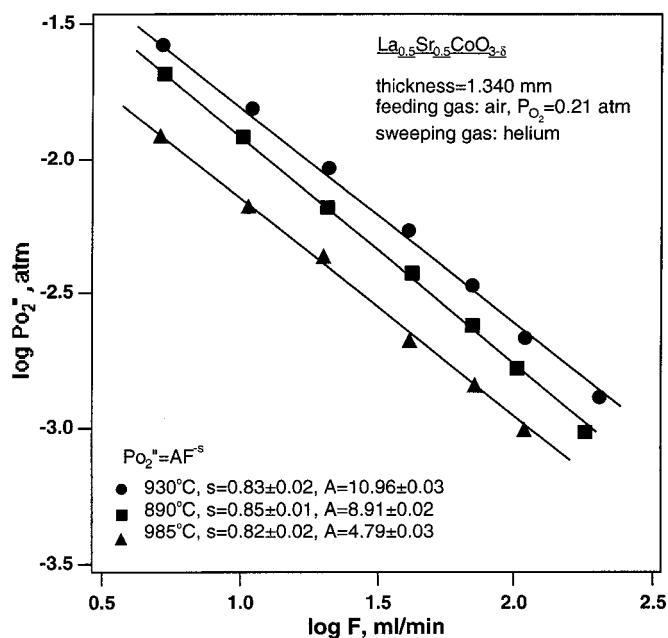


Figure 2. Dependence of p''_{O_2} on flow rate of sweeping helium at different temperatures for $La_{0.5}Sr_{0.5}CoO_{3-\delta}$.

various temperatures show a similar trend, *i.e.*, the rate of increase of p''_{O_2} with p'_{O_2} decreases with increasing p'_{O_2} and decreasing temperature T . The measured p''_{O_2} could be a combined result of oxygen diffusion in the bulk and surface oxygen exchange kinetics at both surfaces. Plots of oxygen flux J_{O_2} vs. the gradient of the partial pressure of oxygen $\log(p'_{O_2}/p''_{O_2})$ at different temperatures reveal a clearer picture (see Fig. 8). An increase in the gradient increases the

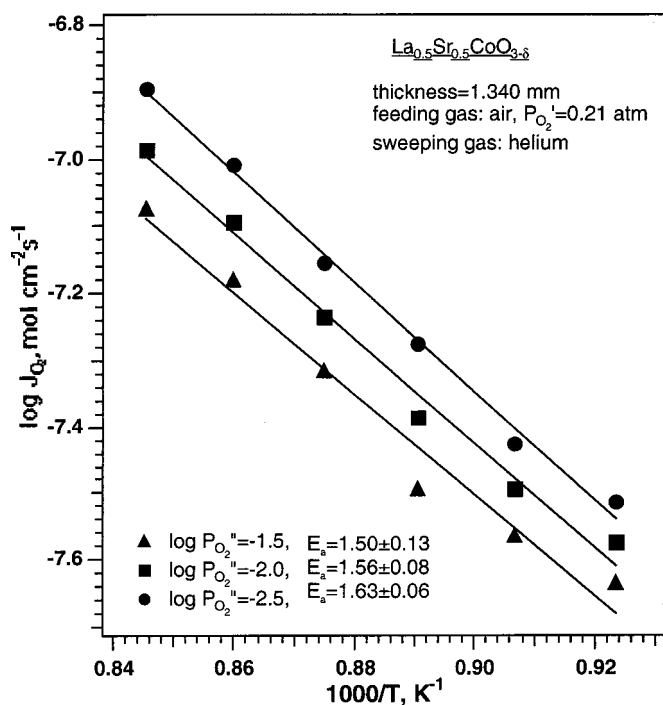


Figure 3. Arrhenius plot of J_{O_2} under a given gradient of chemical potential of oxygen for $La_{0.5}Sr_{0.5}CoO_{3-\delta}$.

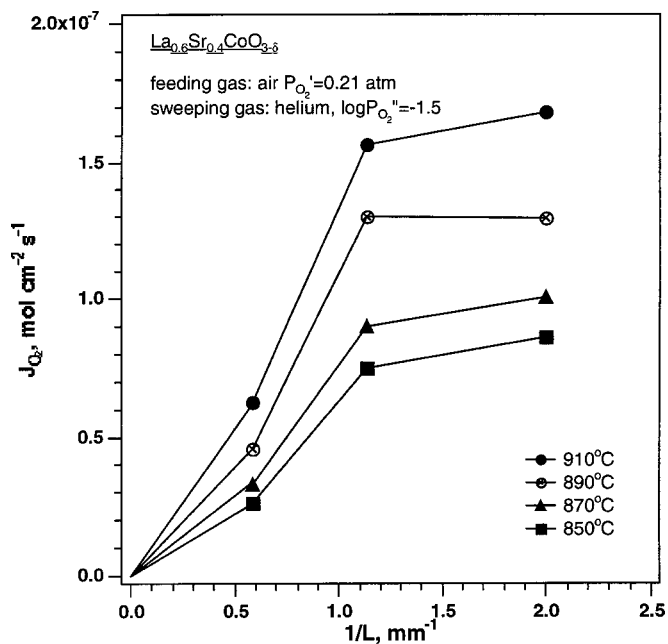


Figure 4. Thickness dependence of J_{O_2} at different temperatures and a given gradient of chemical potential of oxygen for $La_{0.6}Sr_{0.4}CoO_{3-\delta}$.

oxygen flux more effectively at higher temperatures than at lower temperatures. This finding, in turn, implies that the surface reaction kinetics has an activation energy higher than that of bulk oxygen diffusion. In fact, at 800°C, J_{O_2} tends to approach a saturation value with increasing $\log(p'_{O_2}/p''_{O_2})$. As stated above, no linear relationship that passes through (0, 0) can be found in Fig. 8 over the measured T and $\log(p'_{O_2}/p''_{O_2})$ ranges. Nevertheless, plots of J_{O_2} vs. $p'_{O_2} - p''_{O_2}$ (Fig. 9) have been well fitted by straight lines with a 0.5

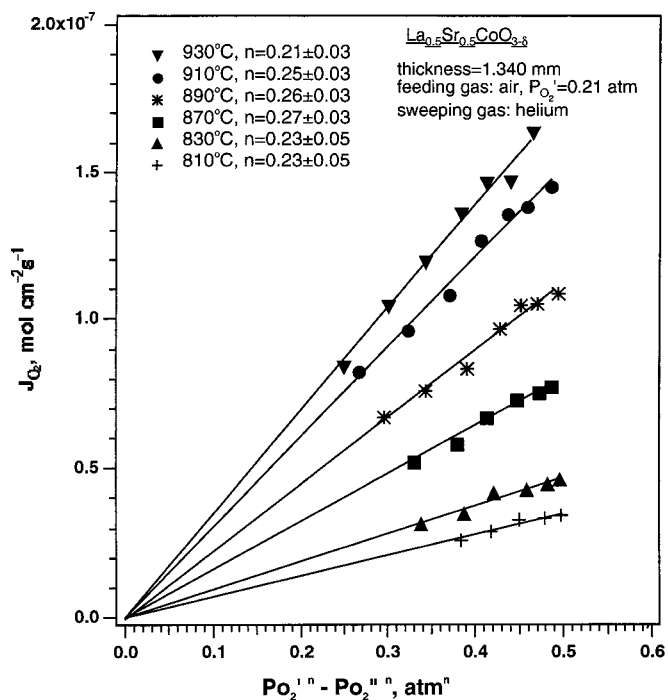


Figure 5. Power law dependence of J_{O_2} on the partial pressure of oxygen for $La_{0.5}Sr_{0.5}CoO_{3-\delta}$.

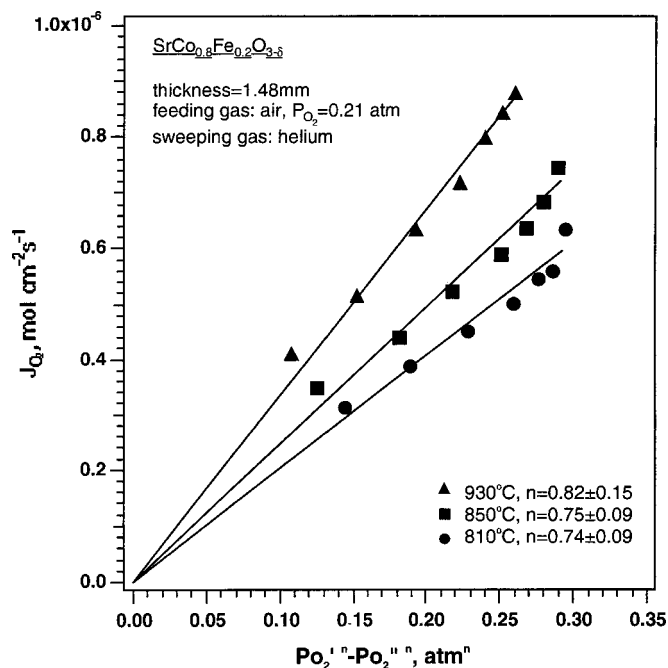


Figure 6. Power law dependence of J_{O_2} on the partial pressure of oxygen for $SrCo_{0.8}Fe_{0.2}O_{3-\delta}$.

$n > 0$ over 800–900°C. According to the model developed in this study, $0.5 > n > 0$ indicates a mixed surface exchange and bulk diffusion of oxygen involved in the overall permeation process. However, in Fig. 9, n is a bit larger at high temperatures than that shown in Fig. 5, although the sample of Fig. 9 is thicker than that of Fig. 5. This result appears to contradict the aforementioned statement that the value of n approaches 0.5 when the sample thickness decreases. Bearing in mind that the partial pressure of oxygen p'_{O_2} in the feeding gas in Fig. 9 varies approximately from 10^{-3} to 1 atm, whereas p'_{O_2} is kept a constant 0.21 atm in Fig. 5, the discrepancy suggests that there is an effect of the partial pressure of oxygen on

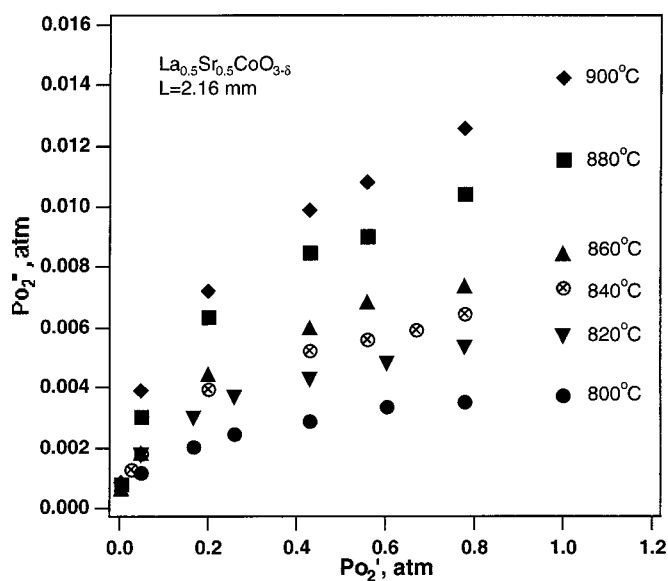


Figure 7. p''_{O_2} as a function of p'_{O_2} at various temperatures. The p'_{O_2} was varied by changing the O_2/N_2 ratio in the feeding gas.

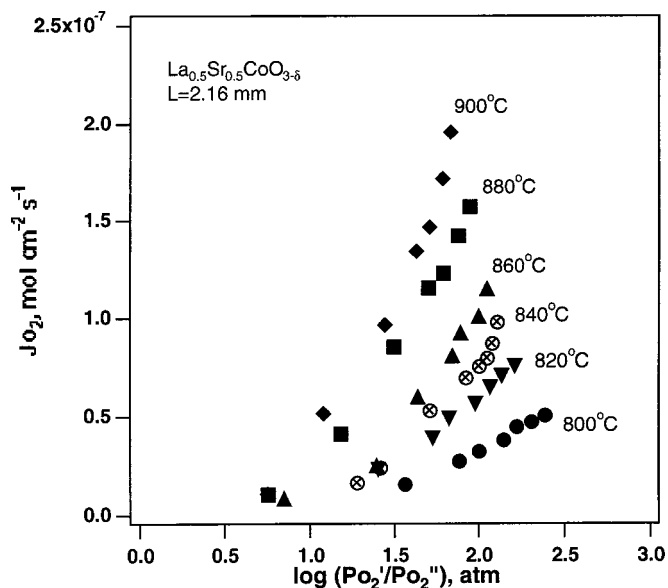


Figure 8. Dependence of J_{O_2} on the gradient of partial pressure of oxygen for $La_{0.5}Sr_{0.5}CoO_{3-\delta}$. The gradient of partial pressure of oxygen was varied as a result of changes of both p'_{O_2} and p''_{O_2} .

the surface kinetics at the feeding-gas side. This assumption is supported in the following section. A logarithmic plot of the slope acquired from Fig. 9 vs. $1/T$ yields an apparent activation energy $E_a = 1.41$ eV, which is comparable to 1.56 eV in Table III for the same but thinner sample.

Oxygen permeation flux J_{O_2} with a catalytic surface layer.— J_{O_2} under $p'_{O_2} = 0.21$ atm and varied p''_{O_2} .—It is expected that a layer of catalytically active SCF coating will promote the surface oxygen

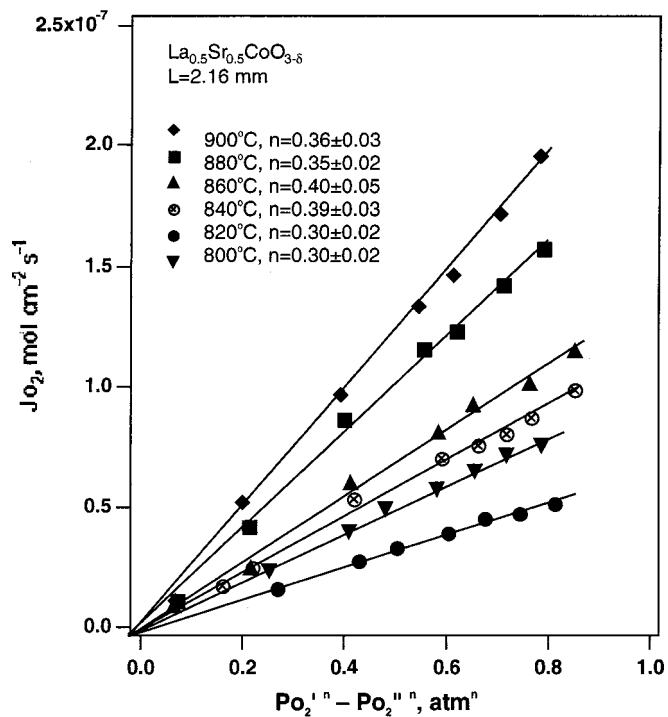


Figure 9. Power law dependence of J_{O_2} on the partial pressure of oxygen for $La_{0.5}Sr_{0.5}CoO_{3-\delta}$ in the case of varied p'_{O_2} and p''_{O_2} .

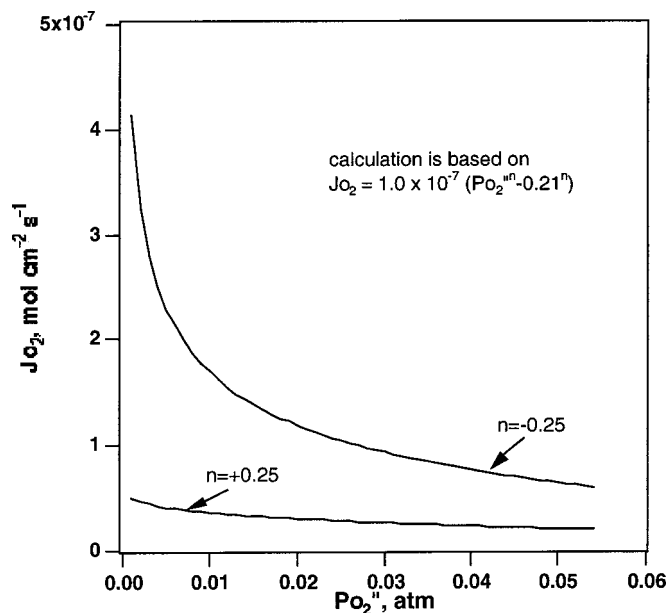


Figure 10. Calculated dependence of J_{O_2} on p''_{O_2} with positive and negative values of n in the relationship $J_{O_2} = 1.0 \times 10^{-7} (p''_{O_2} - 0.21^n)$.

exchange kinetics so that the bulk oxygen diffusion dominates the overall permeation process, thus allowing the bulk transport properties of MIECs to be evaluated. With the assumption of a power law relation between J_{O_2} and p_{O_2} , the dependence of J_{O_2} on p''_{O_2} shown in Fig. 10 was calculated. Clearly, the J_{O_2} exhibits a more remarkable increase at lower p_{O_2} with a negative value of n than that with a positive value of n . This observation, in turn, implies a permeation process dominated by bulk oxygen diffusion, provided a sharp increase of J_{O_2} is found at low p_{O_2} . Representative plots at 810°C of measured J_{O_2} vs. p''_{O_2} with an SCF coating on the feeding-gas side,

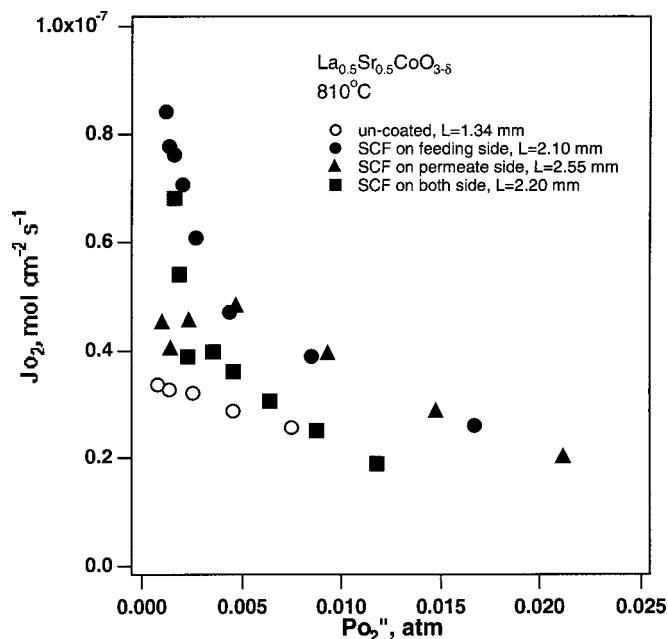


Figure 11. Measured dependence of J_{O_2} on p''_{O_2} at 810°C for uncoated and SCF-coated $La_{0.5}Sr_{0.5}CoO_{3-\delta}$.

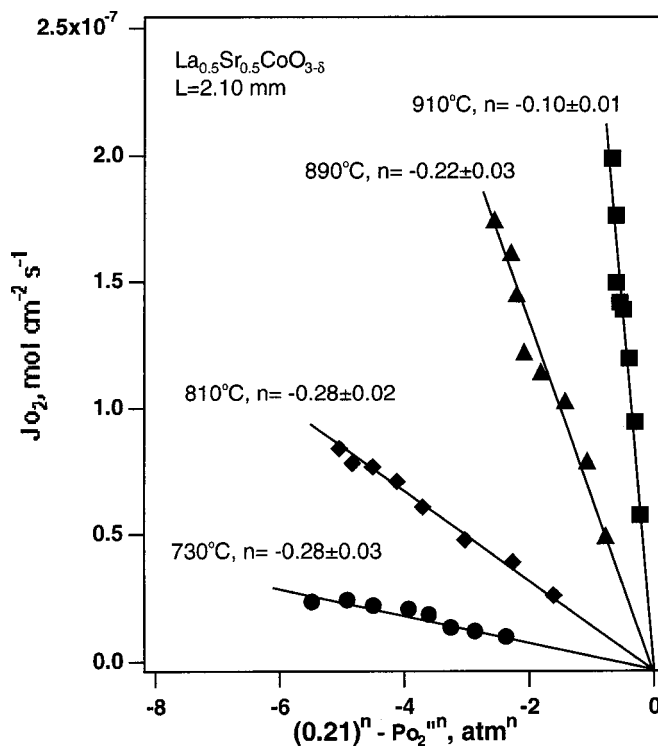


Figure 12. Power law dependence of J_{O_2} on the partial pressure of oxygen for $La_{0.5}Sr_{0.5}CoO_{3-\delta}$ with an SCF coating on the feeding-gas side. The p'_{O_2} at the feeding-gas side was kept constant at 0.21 atm.

sweeping-gas side, and both sides, respectively, are shown in Fig. 11; they are compared to the one obtained without an SCF coating. With a coating on the feeding-gas side, the curve exhibits a very similar shape to that shown in Fig. 10 for $n < 0$, whereas the J_{O_2} without an SCF coating has a fairly flat change with p''_{O_2} . A plot of J_{O_2} vs. $p''_{O_2} - p''_{O_2}^n$, shown in Fig. 12, indeed revealed straight lines with negative values of n at various temperatures. All these observations indicate a changeover of the permeation rate from domination by surface exchange to bulk diffusion after an SCF coating was added on the feeding-gas side at a $p'_{O_2} = 0.21$ atm. However, the curve obtained with an SCF coating on the permeate side, shown in Fig. 11, gives a different trend; a plateau of J_{O_2} occurs below a certain lower p''_{O_2} . Attempts to plot J_{O_2} vs. $p''_{O_2} - p''_{O_2}^n$ for an SCF coating at the permeation side gave a linear relation with negative values of n at higher p''_{O_2} , but a small plateau at lower p''_{O_2} . Previous studies^{20,28} have shown that the brownmillerite phase $Sr_2Co_2O_5$ ^c is favored at lower temperatures and lower partial pressure of oxygen. Therefore, it is reasonable to believe that the small plateau shown in Fig. 11 is caused by the formation of the poorly conducting brownmillerite phase. The curve for an SCF coating on both sides appears, reasonably, to be a combination of the above two situations. A rapid increase of J_{O_2} after a plateau is observed.

The J_{O_2} as a function of the gradient of the partial pressure of oxygen $(1/L)\log(p''_{O_2}/0.21)$ at a given temperature, where L is the thickness of the membrane, is plotted in Fig. 13 for SCF-coated and uncoated samples. Comparison of the 890 and 810°C curves of Fig. 13a and b shows that the J_{O_2} of the SCF-coated samples has been enhanced at both higher and lower temperatures compared to that of the uncoated one. The enhancement is not only a function of tem-

^c Note that the brownmillerite phase could also be $Sr_2Co_{2-x}Fe_xO_5$, according to Ref. 21.

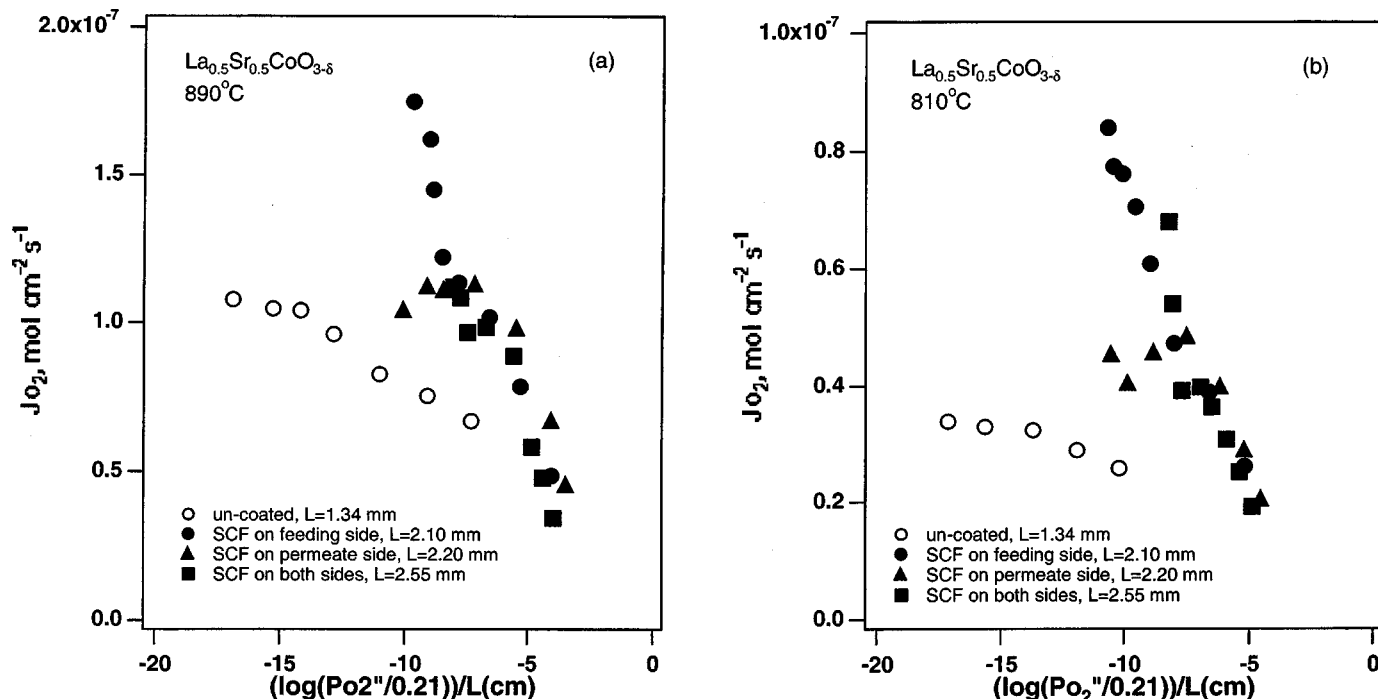


Figure 13. Dependence of J_{O_2} on the gradient of partial pressure of oxygen for uncoated and SCF-coated $\text{La}_{0.5}\text{Sr}_{0.5}\text{CoO}_{3-\delta}$. The $p'_{O_2} = 0.21$ atm was kept constant; (a) 890°C, (b) 810°C.

perature, but is also dependent on the gradient of the partial pressure of oxygen. At a small oxygen gradient or high p''_{O_2} range, the SCF coating appears to be less effective than at a large gradient or low p''_{O_2} range. This may be due to a slower bulk diffusion at a smaller p_{O_2} gradient. However, a slightly higher J_{O_2} with SCF coated on the permeate side at a small oxygen gradient (see Fig. 13a, b) indicates that the generation of oxygen vacancies at the permeate side is enhanced to a limited extent. With decreasing p''_{O_2} at the permeate side (by increasing the flow rate of the sweeping helium gas), the SCF coating on the feeding-gas side gains effectiveness in increasing the J_{O_2} , whereas the SCF at the permeate side has no effect, primarily due to the formation of the brownmillerite phase. The SCF coatings have a more pronounced effect at lower temperatures than at higher temperatures. This observation confirms the statement that the sur-

face oxygen exchange kinetics is slower at lower temperatures than at higher temperatures. In other words, the surface oxygen exchange kinetics requires a higher activation energy than oxygen bulk diffusion.

The changeover of control of permeation rates to bulk oxygen diffusion allows one to calculate the oxide-ion conductivity of a MIEC from the permeation data by differentiating the Wagner equation (Eq. 1) into the following form

$$\sigma_{\text{ambi}} = -\frac{16F^2L}{2.303RT} \left(\frac{\partial J_{O_2}}{\partial \log p''_{O_2}} \right)_{p'_{O_2}=0.21} \quad [2]$$

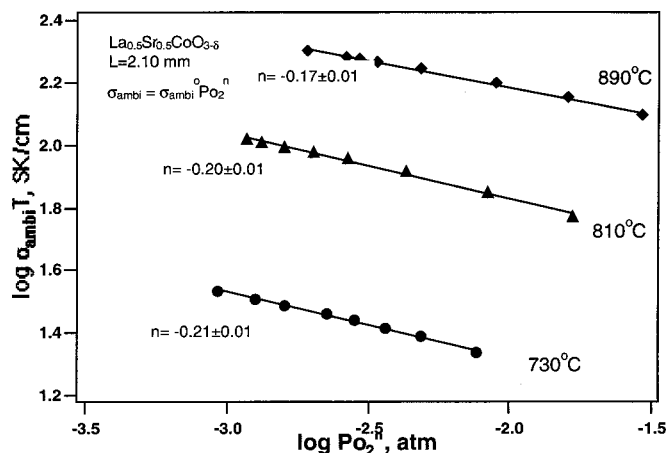


Figure 14. Logarithmic dependence of the ambipolar conductivity of $\text{La}_{0.5}\text{Sr}_{0.5}\text{CoO}_{3-\delta}$ on the partial pressure of oxygen at various temperatures.

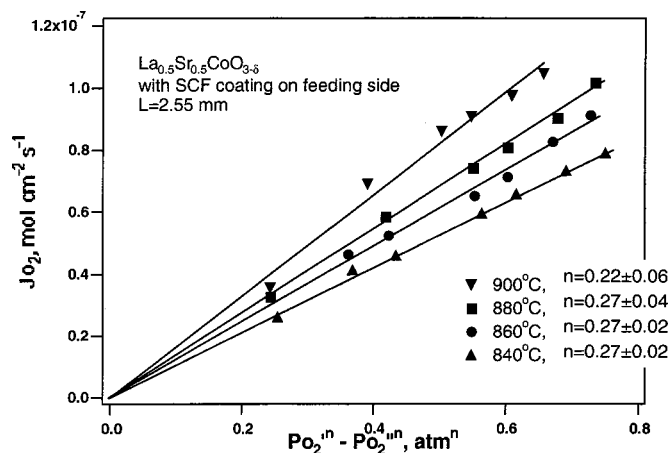


Figure 15. Power law dependence of J_{O_2} on the partial pressure of oxygen for $\text{La}_{0.5}\text{Sr}_{0.5}\text{CoO}_{3-\delta}$ with an SCF coating on the feeding-gas side in the case of varied p'_{O_2} and p''_{O_2} .

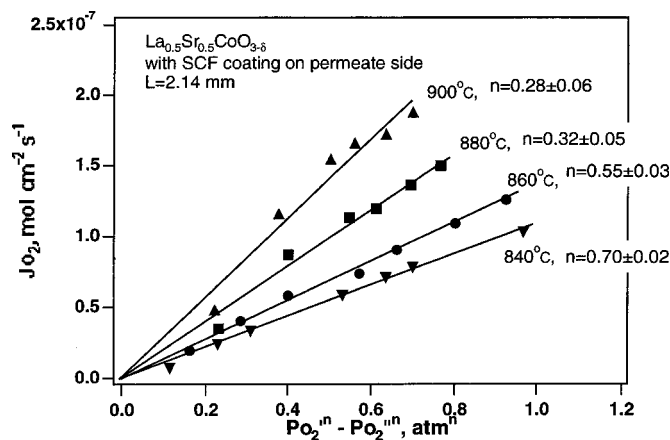


Figure 16. Power law dependence of J_{O_2} on the partial pressure of oxygen for $\text{La}_{0.5}\text{Sr}_{0.5}\text{CoO}_{3-\delta}$ with an SCF coating on the permeate side in the case of varied p'_{O_2} and p''_{O_2} .

where $\sigma_{\text{ambi}} \approx \sigma_{\text{O}}$ as the electronic transport number t_e is far greater than that of the oxide-ion t_{O} in this study. Figure 14 shows the logarithmic dependence of the calculated ambipolar conductivity on the partial pressure of oxygen at different temperatures from the fitted relationship between J_{O_2} and $\log(p''_{O_2})$. The increased oxygen vacancy concentration with decreasing partial pressure of oxygen leads to an increase of the ambipolar conductivity in an MIEC. The power index ranges from -0.17 at 890°C to -0.21 at 730°C , which is reasonably between the $-1/6$ to $-1/4$ predicted from the defect model. The activation energy $E_a = 1.25$ eV for the ambipolar conduction was obtained from the Arrhenius plot of the J_{O_2} .

J_{O_2} under varied p'_{O_2} and fixed sweeping-gas flow rate.—The same permeation cell configurations were used for the measurement of J_{O_2} vs. varied p'_{O_2} and p''_{O_2} . The results are strikingly contrary to those discussed in the section on J_{O_2} under $p'_{O_2} = 0.21$ atm and varied p''_{O_2} . Figure 15 clearly shows little change of n from Fig. 9 after a surface catalytic layer of SCF was applied on the feeding-gas side. The value of n , $0 < n < 0.5$, obtained from the nonlinear least-squares fitting remained essentially the same within the range of $840^\circ\text{C} \leq T \leq 900^\circ\text{C}$. Compared to the sample of Fig. 9 where no SCF coating was applied, the n value is smaller even though the

sample of Fig. 9 has a larger membrane thickness. The coating has some catalytic effect on the surface oxygen exchange on the feeding-gas side at lower temperature (see Fig. 17b). However, it is not so effective as to allow the bulk oxygen diffusion to be the slowest step in the overall serial permeation process since a slow surface reaction due to a relatively low flow rate on the permeate side persisted in dominating the permeation. A positive value of n was also observed with an SCF coating on the permeate side (see Fig. 16), but a significant increase of n values from $0 < n < 0.5$ to a $0.5 < n < 1$ was found below 860°C . These results indicate that the SCF on the permeate side has little catalytic effect and, in fact, lowers the permeation rate below 860°C because of formation of the brownmillerite phase at lower p''_{O_2} . This observation is consistent with the measurement in the preceding section showing that the SCF layer on the permeate side does not effectively increase the exchange kinetics on that surface due to brownmillerite formation.

Comparisons of J_{O_2} for SCF-coated and uncoated samples as a function of $(1/L)\log(p'_{O_2}/p''_{O_2})$ at a given temperature are shown in Fig. 17. At 880°C , Fig. 17a, no catalytic effect was observed with SCF coatings over the entire oxygen gradient range. However, with the temperature lowered to 840°C , Fig. 17b, the J_{O_2} for a sample with SCF coated on the feeding-gas side is higher than that for the uncoated sample. This observation again confirms that surface oxygen exchange kinetics is slower at lower temperatures. The SCF coating on the permeate side appears to have less influence on the J_{O_2} as a result of forming the brownmillerite phase. The J_{O_2} at 840°C is lower than that of the uncoated sample at a low feeding-gas p'_{O_2} range; it rapidly approaches the same value as that of the uncoated sample at higher p'_{O_2} , where a higher p''_{O_2} can be achieved.

From the results of SCF coating at the permeate side shown in these last two sections, it is clear that the formation of a brownmillerite phase at lower p''_{O_2} makes an SCF coating ineffective as a catalyst.

Mechanisms for both surface oxygen exchange and bulk oxygen diffusion control.—A similar study concerning both surface reaction and bulk diffusion associated with the semipermeability of the calcia-doped zirconia was demonstrated by Dou *et al.*²⁷ Unlike pure oxide-ion electrolytes, it is more complicated for mixed electronic and oxide-ion conductors because both oxygen vacancy and hole concentrations could depend on the partial pressures of oxygen. Therefore, the obtained analytic expressions can only be resolved by numerical calculations if no assumptions are made to simplify them. According to the power index $0.5 > n > 0$ obtained for the

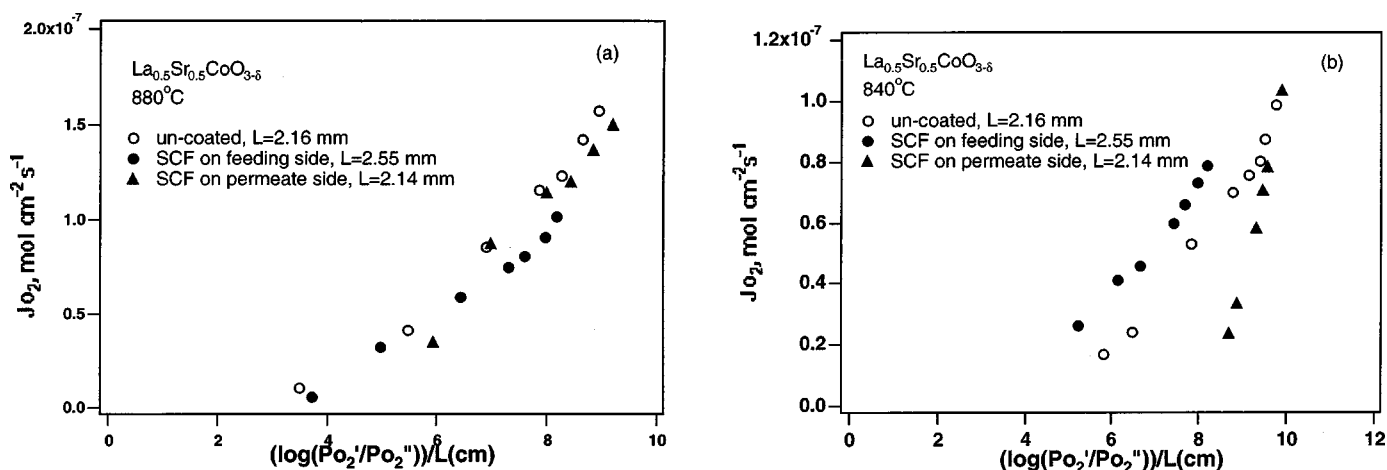
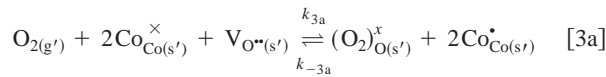
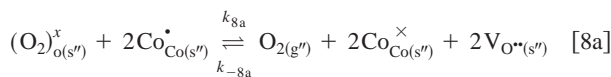
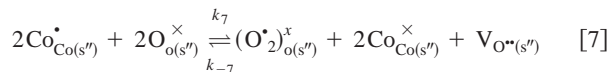
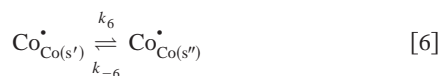
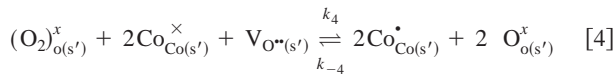
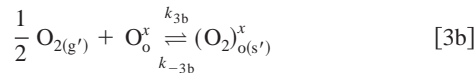


Figure 17. Dependence of J_{O_2} on the gradient of partial pressure of oxygen for uncoated and SCF-coated $\text{La}_{0.5}\text{Sr}_{0.5}\text{CoO}_{3-\delta}$. The p'_{O_2} and p''_{O_2} were both varied; (a) 880°C , (b) 840°C .

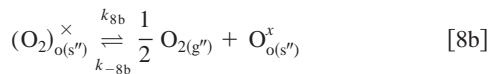
La_{1-x}Sr_xCoO_{3-δ} system, we propose the following mechanism to illustrate the overall permeation process (Kröger-Vink notation is used)



or



or



In the above reactions, k_i and k_{-i} are the rate constants of the forward and reverse reactions, respectively. By the Kröger-Vink notation, O_o^{\times} and $\text{V}_{\text{O}}^{\bullet}$ are a lattice oxygen and an oxygen vacancy, respectively; $\text{Co}_{\text{Co}}^{\times}$ and $\text{Co}_{\text{Co}}^{\bullet}$ are 3+ and 4+ Co ions, respectively; $(\text{O}_2)_{\text{O}}^{\times}$ represents the peroxide ion on the oxygen site; and s' and s'' denote the surfaces at the feeding-gas side and that at the sweeping-gas side, respectively. Reactions 3b and 8b represent the adsorption and desorption of gaseous oxygen to form and to dissociate the peroxide ions on the surface. Many studies have shown the existence of the peroxide ion on the surface of oxides by X-ray photoemission spectroscopy. Reactions 4 and 7 illustrate the annihilation and production of oxygen vacancies that are charge-compensated by electronic holes and electrons, respectively. Over the whole process, we assume that Reactions 3b and 8b as well as electronic transport (Reaction 6) are rapid and at their equilibrium. The rate-determining steps are therefore the transport of surface oxygen atoms to oxygen vacancies (Reaction 4), the production of oxygen vacancies (Reaction 7), and bulk oxygen vacancy diffusion (Reaction 5), dressed by two electrons.

The detailed formulation of the above processes is not given, for conciseness, but the finalized expression is introduced as follows

$$J_{\text{O}_2} = \frac{D_{\text{O}}K_{3b}K_4}{2L} [\text{Co}_{\text{Co}}^{\times}] \frac{\delta^{\circ}}{p^{\circ}} (p_{\text{O}_2}^{\prime 0.5-m-2r} - p_{\text{O}_2}^{\prime\prime 0.5-m-2r})$$

$$[\text{V}_{\text{O}(s')}^{\bullet}] = \delta^{\circ} p_{\text{O}_2}^{\prime -m} \quad [\text{V}_{\text{O}(s'')}^{\bullet}] = \delta^{\circ} p_{\text{O}_2}^{\prime\prime -m} \quad (m > 0) \quad [9]$$

$$[\text{Co}_{\text{Co}(s')}^{\bullet}] = p^{\circ} p_{\text{O}_2}^{\prime r} \quad [\text{Co}_{\text{Co}(s'')}^{\bullet}] = p^{\circ} p_{\text{O}_2}^{\prime\prime r} \quad (r > 0)$$

$$[\text{Co}_{\text{Co}}^{\times}] \approx [\text{Co}_{\text{Co}(s')}^{\times}] \approx [\text{Co}_{\text{Co}(s'')}^{\times}] \approx 1$$

where D_{O} is the oxygen vacancy diffusivity, L is the thickness of the membrane, $[\text{defect}]$ represents the concentration of the defect, δ° and p° are the constants, and K_{3b} and K_4 represent the equilibrium constants of Reactions 3 and 4, respectively.

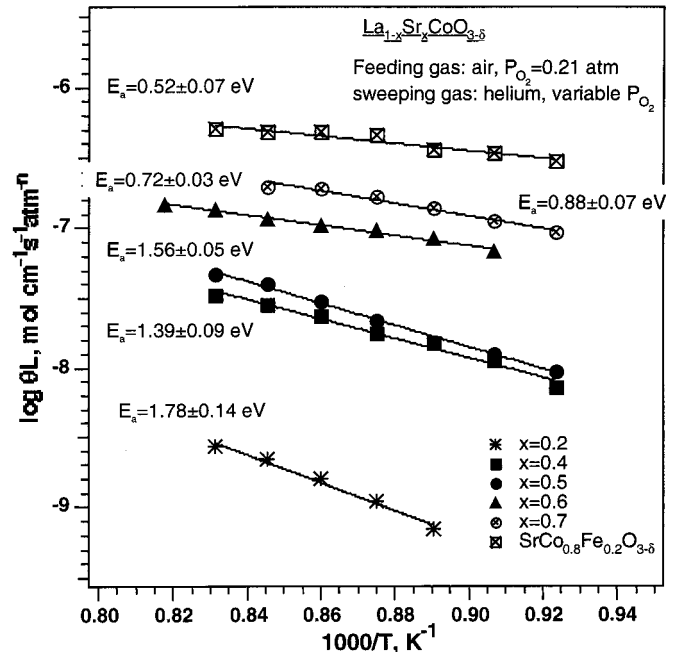


Figure 18. Arrhenius plot of $\log \theta L$ for all uncoated compositions investigated in this study.

For a similar sample thickness at which both surface exchange and bulk diffusion control the permeation, various Sr doping levels could lead to a systematic change of the value of n . Generally, at a lower doping level x , the nonstoichiometry of oxygen is very low, and the electrical neutrality condition may be simplified into $p \approx x$, in which case $n = 0.5 - m$ in Eq. 9. At a higher Sr doping x , the nonstoichiometry of oxygen could be fixed by Sr doping, and the electrical neutrality condition can be simplified to $\delta = x/2$, and $n = 0.5 - 2r$ in Eq. 9. At intermediate doping, a minimum of $n = 0.5 - m - 2r$ can be expected. The experimental data in Table III confirm such a prediction.

For the $\text{SrCo}_{0.8}\text{Fe}_{0.2}\text{O}_{3-\delta}$ sample, the $1 > n > 0.5$ shown in Table III appears to imply a different rate-limiting step at the surfaces. We notice that Fe may play a decisive role in the surface reaction since a surface Fe^{3+} ion is stable in tetrahedral coordination. As in Reaction 3a, gaseous oxygen occupies the site of an oxygen vacancy on the surface to become a surface peroxide ion. However, at an Fe^{3+} ion, transformation from tetrahedral to octahedral oxygen coordination allows the gaseous O_2 to become 2O^{2-} without surface diffusion of oxygen to a vacancy at another cation. Therefore, Reactions 3a and 8a become rate limiting. The oxygen flux J_{O_2} is given in the following equation

$$J_{\text{O}_2} = \varepsilon (p_{\text{O}_2}^{\prime 1-m} - p_{\text{O}_2}^{\prime\prime 1-m}) \quad (m > 0) \quad [10]$$

$$\varepsilon = \frac{1}{2} k_{-3a} [\text{Co}_{\text{Co}}^{\times}] \delta^{\circ}$$

where the power index $n = 1 - m$ is obtained. k_{-3a} represents the rate constant of the reverse reaction (Reaction 3a). This prediction agrees well with the experimental data shown in Table III.

According to Eq. 9, $\log \theta L$ vs. $1/T$ should give a straight line with a slope associated with the apparent activation energy E_a of the permeation process, where θ represents the slope of the straight line obtained by plotting J_{O_2} vs. $p_{\text{O}_2}^{\prime n} - p_{\text{O}_2}^{\prime\prime n}$. Figure 18 presents such a

plot for all compositions studied as indicated by Eq. 9. The shown activation energies E_a exhibit a general decrease with Sr doping level x . If E_a for $x = 0.20$ represents the bulk diffusion, the highest E_a signals an unfavorable migration environment due to the presence of two electronic phases.²⁵ However, with increasing doping level x , both structure and oxygen vacancy concentration begin to favor high oxygen conductivity, which changes the rate-limiting step from bulk diffusion to surface exchange. Provided that surface exchange does not change very much with composition, the significant decrease of activation energy E_a must be attributed to the change of the structure and oxygen vacancy concentration. It is clear that cubic symmetry that leads to a linear configuration of the Co-O-Co bonds in the perovskite is the best structure for having the highest oxide-ion mobility. In the rhombohedral structure, the Co-O bonds are under compression. In the cubic structure, the Co-O bonds are under tension, and the tension increases with temperature because of the larger thermal expansion of the A-O bonds of an ACoO₃ perovskite where there is no low-spin to intermediate-spin transition on the Co(III). Comparison of La_{1-x}Sr_xCoO_{3-δ} and SrCo_{0.8}Fe_{0.2}O_{3-δ} illustrates a trend to lower activation energy as the stress on the Co-O bond changes.

Conclusions

The oxygen flux J_{O_2} across two ceramic membranes, SrCo_{0.8}Fe_{0.2}O_{3-δ} and La_{0.5}Sr_{0.5}CoO_{3-δ} as a representative of the La_{1-x}Sr_xCoO_{3-δ} system, were systematically studied as a function of temperature, the gradient of oxygen chemical potential, and thickness. The gradient of oxygen partial pressure across a membrane was varied either by changing the p''_{O_2} at the permeate side with a fixed $p'_{O_2} = 0.21$ atm at the feeding-gas side or by changing the feeding-gas p'_{O_2} while keeping constant the flow rate of a helium sweeping gas at the permeate side. The influence of a catalytically active surface layer SrCo_{0.8}Fe_{0.2}O_{3-δ} on the J_{O_2} of La_{0.5}Sr_{0.5}CoO_{3-δ} was also studied.

The magnitude of p''_{O_2} varies as a power of the rate of flow of the helium sweeping gas across the permeate surface, and the power index is independent of temperature. As a consequence, plots of J_{O_2} vs. $(p'_{O_2} - p''_{O_2})^n$ for a fixed membrane thickness L were straight lines passing through the origin with a slope varying as $L^{-1} \exp(-E_a/kT)$. The temperature dependence of J_{O_2} under a given $\log(p'_{O_2}/p''_{O_2})$ and L was shown to obey an Arrhenius relation with an activation energy $E_a = 1.56$ eV for La_{0.5}Sr_{0.5}CoO_{3-δ} without an active SCF coating, and a positive power index $0.5 > n > 0$ showed that the oxygen flux across the membrane is controlled partially by the reaction kinetics at the surface. The value of n increased with decreasing membrane thickness toward a predicted 0.5 for surface control. For SrCo_{0.8}Fe_{0.2}O_{3-δ}, the value of n was in the range of $1 > n > 0.5$, which indicates that a surface reaction different from that on La_{0.5}Sr_{0.5}CoO_{3-δ} is rate controlling.

With a catalytically active SCF coating, the dependence of J_{O_2} on the gradient of the partial pressure of oxygen and the temperature can be used to determine the rate-limiting steps by comparison with the data for an uncoated sample. At a fixed $p'_{O_2} = 0.21$ atm, the J_{O_2} can be remarkably increased at a lower p''_{O_2} with a coat of the SCF on the feeding-gas side. In contrast, an SCF coating on the permeate side has little effect at high p''_{O_2} and even a negative effect on J_{O_2} at low p''_{O_2} due to the formation of a poorly conducting brownmillerite phase. For a fixed helium flow rate of 20 mL/min at the permeate side while changing the p'_{O_2} at the feeding side, the SCF coating does not increase J_{O_2} significantly over the entire partial pressure gradient of oxygen measured. In other words, the SCF coating does not enhance the surface reaction as in the case of a fixed p'_{O_2}

= 0.21 atm and a varied p''_{O_2} . The value of n remained positive, indicating surface-involved rate-limiting steps in the permeation process for all p_{O_2} and temperatures. This observation may imply that the gas flowing pattern is important. However, in both cases, the SCF coating evidently increased the J_{O_2} more at lower temperatures than at higher temperatures, which signals that the overall exchange kinetics requires a higher activation energy than that of ambipolar transport across the MIEC.

Another important finding in this study is the changeover of the rate-limiting step from surface or surface-bulk mixed control to a sole bulk control with the aid of an SCF coating on the feeding-gas side. This changeover enabled us to evaluate the bulk properties of the MIEC. The ambipolar conductivity for the La_{0.5}Sr_{0.5}CoO_{3-δ} follows a power law relationship with p_{O_2} ; the power index ranges from $n = -0.17$ at 890°C to -0.21 at 730°C. The Arrhenius plot of the ambipolar conductivity gave an activation energy $E_a = 1.25$ eV under a $p_{O_2} = 0.01$ atm.

Two mechanistic models were proposed to interpret the observed results in the systems La_{1-x}Sr_xCoO_{3-δ} and SrCo_{0.8}Fe_{0.2}O_{3-δ}. For the La_{1-x}Sr_xCoO_{3-δ} system, the transport of surface oxygen to a vacancy on the feeding-gas surface and the creation of oxygen vacancies on the permeate side are assumed to be the rate-determining steps on the surface, while the step that transports an oxygen vacancy is the rate-determining step in the bulk. Based on this model, an expression $J_{O_2} = \theta(p'_{O_2} - p''_{O_2})^n$, where $0.5 > n > 0$, has been derived. For the SrCo_{0.8}Fe_{0.2}O_{3-δ} system, a similar expression can be obtained with $1 > n > 0.5$ by assuming that the chemisorption and desorption of gaseous O₂ on the surfaces are the rate-determining steps. The model agrees well with the experimental results.

Acknowledgments

The authors thank Robert Welch Foundation for financial support. The authors are grateful to Dr. Schöder for his partial help on the setup of the instrument and Jenh-Haw Wan for helping to make some of the samples.

The University of Texas at Austin assisted in meeting the publication costs of this article.

References

1. I. Riess, *Solid State Ionics*, **91**, 221 (1996).
2. I. Riess and D. S. Tannhauser, *Solid State Ionics*, **7**, 307 (1982).
3. B. Ma, J.-H. Park, C. U. Segre, and U. Balachandran, *Mater. Res. Soc. Symp. Proc.*, **393**, 49 (1997).
4. J. Maier, *Solid State Ionics*, **112**, 197 (1998).
5. R. A. De Souza and J. A. Kilner, *Solid State Ionics*, **106**, 175 (1998); **126**, 153 (1999).
6. J. A. Kilner, B. C. H. Steele, and L. Ilkov, *Solid State Ionics*, **12**, 89 (1984).
7. R. J. Chater, S. Carter, J. A. Kilner, and B. C. H. Steele, *Solid State Ionics*, **53-56**, 859 (1992).
8. J. A. Kilner and R. A. De Souza, in *High Temperature Electrochemistry: Ceramics and Metals, Proceedings 17th Int. Riso Symp. Mat. Sci.*, F. W. Poulsen, N. Bonanos, S. Linderoth, M. Morgensen, and B. Zachau-Christiansen, Editors, Roskilde, Denmark, p. 41, 1996.
9. J. A. Kilner, in *Proceedings of the Second International Symposium on Ionic and Mixed Conducting Ceramics*, T. A. Ramanarayanan, W. L. Worrell, and H. L. Tuller, Editors, PV 94-12, p. 174, The Electrochemical Society Proceedings Series, Pennington, NJ (1994).
10. C. H. Chen, H. Kruidhof, H. J. M. Bouwmeester, and A. J. Burggraaf, *J. Appl. Electrochem.*, **27**, 71 (1997).
11. C. H. Chen, H. J. M. Bouwmeester, R. H. E. van Doorn, H. Kruidhof, and A. J. Burggraaf, *Solid State Ionics*, **98**, 7 (1997).
12. R. H. E. van Doorn, H. Kruidhof, H. J. M. Bouwmeester, and A. J. Burggraaf, *Mater. Res. Soc. Symp. Proc.*, **369**, 377 (1995).
13. B. C. H. Steele, *Solid State Ionics*, **75**, 157 (1995).
14. H. J. M. Bouwmeester, H. Kruidhof, and A. J. Burggraaf, *Solid State Ionics*, **72**, 185 (1994).
15. J. A. Kilner, R. A. De Souza, and I. C. Fullarton, *Solid State Ionics*, **86-88**, 703 (1996).
16. A. Bielanski and J. Haber, *Oxygen in Catalysis*, Marcel Dekker, New York (1991).
17. M. Misono and T. Nitadori, in *Adsorption and Catalysis on Oxide Surfaces*, M. Che and G. C. Bond, Editors, p. 409, Elsevier, Amsterdam (1985).

18. M. Pechni, U.S. Pat. 3,330,697 (1967).
19. K. Q. Huang and John B. Goodenough, *Solid State Chem.*, **136**, 274 (1998).
20. L. Qiu, T. H. Lee, L. M. Liu, Y. L. Yang, and A. J. Jacobson, *Solid State Ionics*, **76**, 321 (1995).
21. W. T. A. Harrison, T. H. Lee, Y. L. Yang, D. P. Scarfe, L. M. Liu, and A. J. Jacobson, *Mater. Res. Bull.*, **30**, 621 (1995).
22. H. Ohbayashi, T. Kudo, and T. Gejo, *Jpn. J. Appl. Phys.*, **13**, 1 (1974).
23. J. Mizusaki, Y. Mima, S. Yamauchi, and K. Fueki, *Solid State Chem.*, **80**, 102 (1989).
24. A. N. Petrov, V. A. Cherepanov, O. F. Kononchuk, and Ya. Gavrilova, *Solid State Chem.*, **87**, 69 (1990).
25. M. A. Sen̄aris-Rodríguez and J. B. Goodenough, *J. Solid State Chem.*, **118**, 323 (1995).
26. T. H. Lee, Y. L. Yang, A. J. Jacobson, B. Abeles, and M. Zhou, *Solid State Ionics*, **100**, 77 (1997).
27. S. Dou, C. R. Masson, and P. D. Pacey, *J. Electrochem. Soc.*, **132**, 1843 (1985).
28. L. M. Liu, T. H. Lee, L. Qiu, Y. L. Yang, and A. J. Jacobson, *Mater. Res. Bull.*, **31**, 29 (1996).